Journal of Power Sources 218 (2012) 168–173

Contents lists available at SciVerse ScienceDirect

Journal of Power Sources

journal homepage: www.elsevier.com/locate/jpowsour

New functionalized graphene sheets for enhanced oxygen reduction as metal-free cathode electrocatalysts

Mohammad Shamsuddin Ahmed, Seungwon Jeon*

Department of Chemistry and Institute of Basic Science, Chonnam National University, Gwangju 500-757, Republic of Korea

HIGHLIGHTS

► The tridodecylmethylammonium chloride functionalized/adsorbed graphene sheet for ORR.
► Metal-free, methanol/ethanol tolerable and long term stable catalyst in fuel cell application.
► Exhibits four-electron oxygen reduction pathway.

ARTICLE INFO

Article history:
Received 22 May 2012
Received in revised form
13 June 2012
Accepted 17 June 2012
Available online 7 July 2012

Keywords:
Functionalized graphene
Oxygen reduction
Fuel cell
Metal free catalyst

ABSTRACT

Tridodecylmethylammonium chloride (TDMAC) functionalized reduced graphene oxide (TDMAC-RGO) has synthesized by a simple physicochemical process. The resultant functionalized graphene imparts electrocatalytic activity as metal- free catalysts for the oxygen reduction reaction (ORR) in fuel cells (FCs), with long-term operational stability, and tolerance to methanol and ethanol *via* a four-electron pathway in alkaline FCs. The ORR activities have systematically investigated by cyclic voltammetry (CV) and rotating ring disk electrode (RRDE) techniques. The results show that the TDMAC-RGO demonstrates excellent catalytic activity for oxygen reduction. Raman and X-ray photoelectron spectroscopic (XPS) measurements indicate charge transfer from the graphene sheets to the TDMAC *via* intermolecular charge-transfer. TDMAC-RGO catalysts are low-cost, free of metal and costly polymers, and are an efficient approach to FC applications.

1. Introduction

Cathodic oxygen reduction reaction (ORR) is an active area of research due to its crucial role in electrochemical energy conversion in fuel cells (FCs) [1–3]. One of the most attractive challenges in this area is the development of efficient ORR electrocatalysts for application in FCs. Huge effort has been devoted to the study of platinum and platinum-based metal alloy electrocatalysts, because they are the most effective electrocatalyst for ORRs in the cathodes of commercial FCs [4–7]. Though, the platinum-based electrode has faced many troubles with respect to mass marketing FCs for commercial applications, such as its susceptibility to time-dependent drift and carbon monoxide deactivation [8–10], slow electron-transfer kinetics [11], high costs, limited supply [12], and poor durability [13]. Recently, metal-free catalysts have received much attention because of their increased electrocatalytic activity in the ORR and their better activity, long term stability [14], and tolerance to interfering substances [15] for alkaline FCs. A possible contribution of metal impurities to the ORR catalysis cannot be stopped completely.

Graphene sheets are two-dimensional flat lattices consisting of a monolayer of sp^2-hybridized carbon atoms that were discovered by Geims' group in 2004 [16]. This material has attracted great interest in a wide range of fields, especially in sensors [17,18] and ORR catalysts [14,15,19], due to its excellent physical and chemical properties such as high electrical conductivity [20] and high surface area [21]. Dai's group [19] observed ORR catalytic activities of graphene sheets to the electron-accepting ability of the positive charged nitrogen atoms. As a result, a net positive charge is created *via* intramolecular charge-transfer on adjacent carbon atoms in nanocarbon structures that readily attract electrons from the anode for facilitating oxygen (O_2) adsorption and the ORR process.

Presently, graphene sheets have been prepared by a variety of techniques [16,22,23]. Among these methods, chemical reduction of exfoliated graphene oxide (GO) is an efficient approach to large-scale production at low cost, which includes noncovalent and covalent functionalization of reduced graphene oxide (RGO) [24–27]. GO can be functionalized by tridodecylmethylammonium

* Corresponding author. Tel.: +82 62 530 0064; fax: +82 62 530 3389.
E-mail address: swjeon3380@naver.com (S. Jeon).

0378-7753/$ – see front matter © 2012 Elsevier B.V. All rights reserved.
http://dx.doi.org/10.1016/j.jpowsour.2012.06.105

chloride (TDMAC), which is highly soluble in various solvents [28]. A quaternary ammonium salt, TDMAC could create net positive charge on carbon-atoms in a total graphene sheet *via* intermolecular charge transfer (Scheme 1). The resultant TDMAC-functionalized/adsorbed RGO (TDMAC-RGO) has been shown to possess enhanced electrocatalytic activities toward ORR. The adsorption of TDMAC onto the surface of graphene sheets was performed during the process of reducing GO into RGO by sodium borohydride ($NaBH_4$) in the presence of TDMAC [29]. $NaBH_4$ was used as a reducing agent instead of highly toxic and dangerously unstable hydrazine. Comparatively, this supplies an environmentally friendly approach for large-scale production of RGO.

Nitrogen atoms can be introduced into graphene sheets to produce N-doped graphene [30,31] that could interfere with the intermolecular charge-transfer effect through hydrazine reduction. Successive adsorption of TDMAC made the surface of RGO positively charged, leading to good dispersion *via* electrostatic repulsion among individual graphene sheets. For comparison, $NaBH_4$-reduced RGO was prepared in the absence of TDMAC. The color of the suspension changed from the yellow-brown of GO to black for RGO and TDMAC-RGO. Present work has done to obtain good ORR catalysts with low cost, long term active, and tolerance to interfering molecules for alkaline FCs.

2. Experimental

2.1. Synthesis of TDMAC functionalized/adsorbed RGO

GO was synthesized from graphite powder according to a modified Hummers method [31–33]. 10 mg GO was loaded into a 50-mL round bottom flask, followed by the addition of 30 mL of 0.1 M tridodecylmethylammonium chloride (TDMAC) (in water) to produce an inhomogeneous dispersion. This dispersion was sonicated 1 h and kept under stirring for 16 h. Thereafter, 160 ? of 0.1 M $NaBH_4$ (in water) was added and the solution was stirred for 30 min, followed by reflux in a temperature controlled heating mantle at 130°C equipped with a water-cooling condenser for 3.30 h to produce a homogeneous black suspension. The final product, TDMAC-RGO, was collected through filtration and dried for 24 h at 50°C in a vacuum oven. To obtain the unfunctionalized RGO, the above procedure was adopted in the absence of TDMAC.

2.2. Characterizations of physical parameters

FTIR measurements were performed on an FTIR spectroscope (PerkinElmer). Raman spectra were collected with LabRam HR800 UV Raman microscope (Horiba Jobin-Yvon, France), with an excitation wavelength of 514 nm Ar^+ ion laser. X-ray photoelectron spectroscopic (XPS) measurements were performed on a MultiLab 2000 (Thermo Electron Corporation, England) with a 14.9 keV Al K X–ray source.

2.3. Electrochemical measurements

For the electrode preparation, TDMAC-RGO or RGO suspension in ethanol (1 mg mL^{-1}) was prepared by introducing a predetermined amount of the corresponding sample under sonication. A 10 ? portion of the TDMAC-RGO or RGO suspension was then dropped onto the surface of a glassy carbon electrode (GCE, 0.5 cm in diameter) prepolished with 0.05 ? alumina suspension on a polishing cloth (BAS, USA). The ring collection efficiency ($N = 0.18$) was determined using ferrocene solution. All Voltammetric measurements were taken using a three-electrode potentiostat [CHI 700C electrochemical workstation (USA)] in a grounded Faraday cage. Platinum wire was used as an auxiliary electrode. A calibrated Ag/AgCl electrode from Bioanalytical Systems Inc. (BAS) in 3 M NaCl solution was used as a reference electrode. All electrochemical measurements, including cyclic voltammograms (CV), rotating-disk electrode (RDE) voltammograms, rotating ring-disk electrode (RRDE) voltammograms and chronoamperometry, were performed at room temperature in 0.1 M KOH solutions, which were purged with high purity O_2 for at least 30 min prior to each measurement.

3. Results and discussion

The reduction of the oxygen containing groups in GO and the concomitant adsorption of TDMAC onto RGO were followed by FTIR spectroscopy (Fig. 1). The FTIR spectra of GO show a strong absorption band at 1750 cm^{-1} due to C—O stretching, and at around 1,640 cm^{-1} attributable to aromatic C=C. The spectrum of GO also exhibits the presence of O—H (at 1,415 cm^{-1}), and epoxy (at 1,260 cm^{-1}) [19,34]. After the GO is reduced by $NaBH_4$, the characteristic absorption bands of oxide groups (O—H, C=O, and epoxy) decreased dramatically and a strong aromatic C=C absorption band could be observed, indicating that the GO had been successfully reduced. The FTIR spectrum of TDMAC-RGO is characterized by the appearance of new peaks at around 1,076 cm^{-1}, attributable to the C—N (aliphatic amine) bond in the adsorbed TDMAC with C=C absorption band. Multiple absorption bands at 2,939 cm^{-1} and 2,877 cm^{-1} are attributable to the—C—H_n.

Raman spectroscopy is one of the most widely used techniques to characterize the structural and electronic properties of graphene

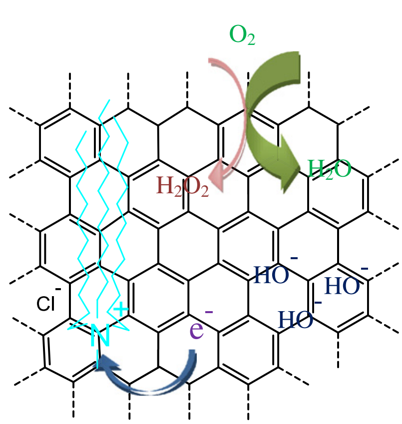

Scheme 1. Schematic Figure showing electron receiving by TDMAC from RGO sheet for enhancing the ORR and O_2 reduced to H_2O as a main product.

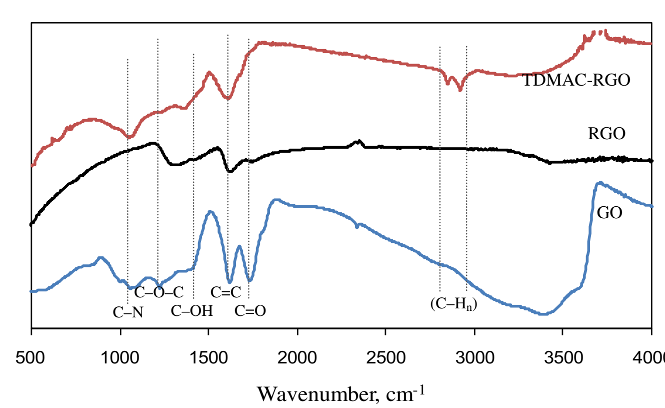

Fig. 1. The FTIR spectra of GO, RGO and TDMAC-RGO.

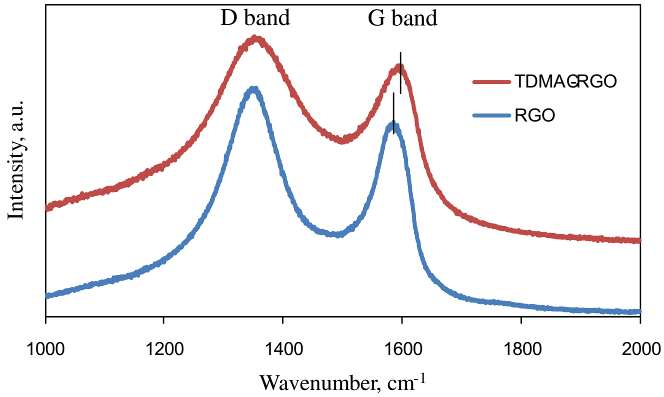

Fig. 2. Raman spectra of RGO and TDMAC functionalized RGO.

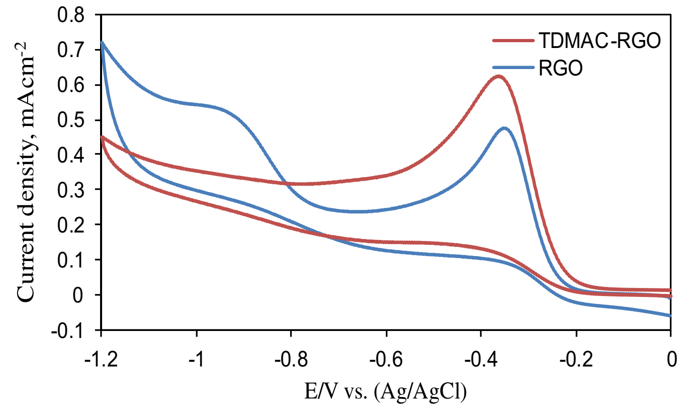

Fig. 4. CVs of oxygen reduction on the RGO and TDMA functionalized RGO in O_2-saturated 0.1 M KOH at a scan rate of 50 mV s^{-1}.

sheets including doping level. In many cases, the Raman spectrum of graphene sheets is characterized by two main features, the G mode arising from the first order scattering of the E_{2g} phonon of sp^2 C atoms, and the D mode arising from a breathing mode of -point photons of A_{1g} symmetry. In the typical Raman spectrum of RGO (Fig. 2), the G band is attributable to 1,586 cm^{-1} and D band is attributable to 1,349 cm^{-1}. The ratio of D/G intensity slightly increased from GO to RGO, due to a decrease in the size of the in-plane sp^2- domain induced by the $NaBH_4$ reduction [33]. After its reduction with TDMAC, the Raman spectrum of TDMAC-RGO also exhibits the presence of D bands at 1,349 cm^{-1}, but the G band shifted from 1,586 cm^{-1}–1,594 cm^{-1} due to electron transfer from graphene sheets to the adsorbed TDMAC [35]. Similar G-band shifts caused by charge-transfer have been reported for graphene sheets functionalized with other electron-accepting molecules [36].

The elemental compositions and charge transfer from graphene sheets were further investigated using XPS. Fig. 3a shows that the XPS spectra of GO and RGO show the presence of only carbon and oxygen atoms. The O/C atomic concentration ratio drastically decreased after the $NaBH_4$ reduction. The following TDMAC functionalization caused further decrease in the O/C atomic concentration ratio, which was accompanied by the appearance of N 1s and Cl 2p peaks located around 401.8 and 199.4 eV, respectively. The high-resolution C 1s XPS spectra for GO, RGO, and TDMAC-RGO are shown in Fig. 3b. The binding energy of 284.9 eV is attributable to the C—C and C═C bonds. The peaks located at the binding energies of 286.3, 287.6, and 289.2 eV are assigned to the C—O, C═O, and O═C—O oxygen-containing functional groups, respectively [37,38]. The spectra of RGO and TDMAC-RGO show a significant reduction of oxygen-containing groups compared to the GO, indicating efficient reduction of the GO by $NaBH_4$. Fig. 3c reveals the N 1s core level XPS spectra of the pristine TDMAC and TDMAC-RGO. While the peak at 402.1 eV for the pristine TDMAC is attributable

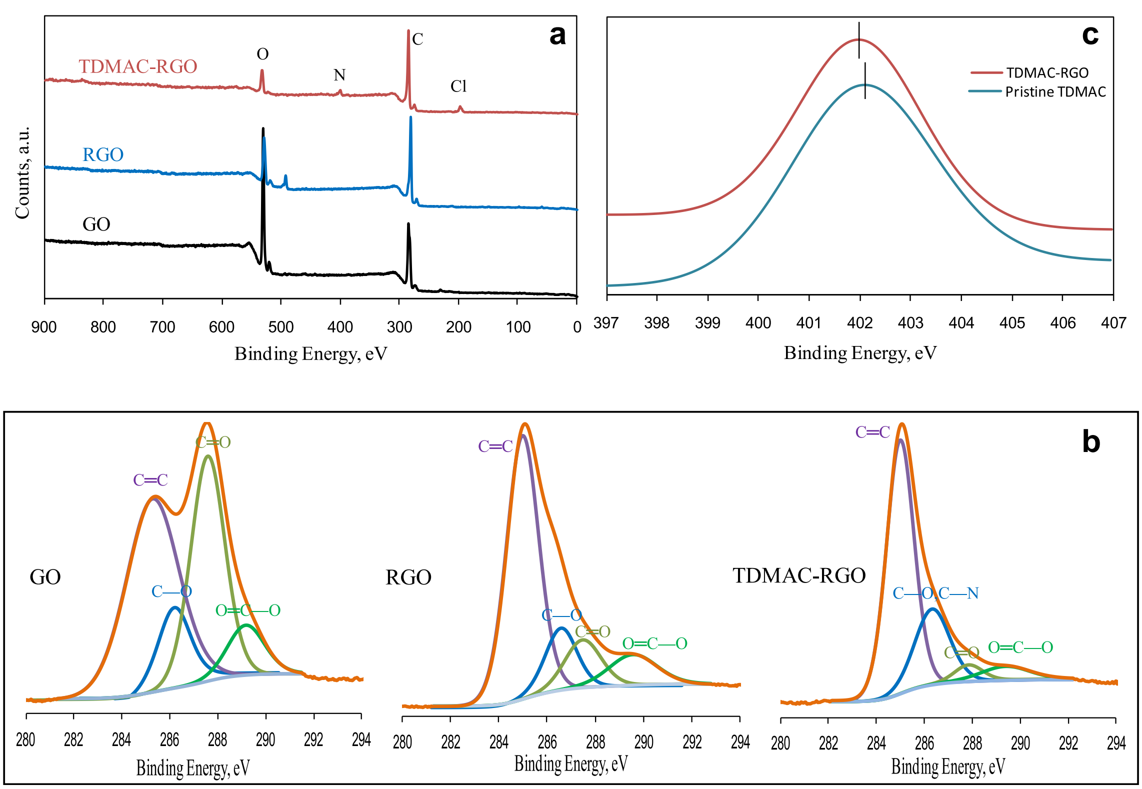

Fig. 3. (a) XPS survey spectra for GO, RGO, and TDMAC-RGO. The core level XPS spectra of C 1s of (b) GO, RGO, and TDMAC-RGO. (c) The core level N 1s XPS spectra of TDMAC-RGO and pristine TDMAC.

to the quaternary nitrogen [19], its negative shift to a lower binding energy at 401.7 eV in TDMAC-RGO indicates electron transfer from graphene sheets to the positively charged TDMAC [39,40].

To investigate the electrocatalytic activities toward ORR of the TDMAC functionalized RGO catalyst compared to RGO, cyclic voltammograms were measured in O_2- saturated 0.1 M KOH solutions at a constant active mass loading onto a glassy carbon electrode (GCE). As can be observed from Fig. 4, distinct peaks corresponding to ORR can be found for RGO- and TDMAC-RGO-modified electrodes. A cathodic reduction peak is displayed in an O_2-saturated solution for the RGO electrode. After the functionalization of TDMAC, the onset potential of the ORR for the TDMAC-RGO electrode shifted positively with a more pronounced increase in current density. This result clearly indicates that the ORR catalytic activity

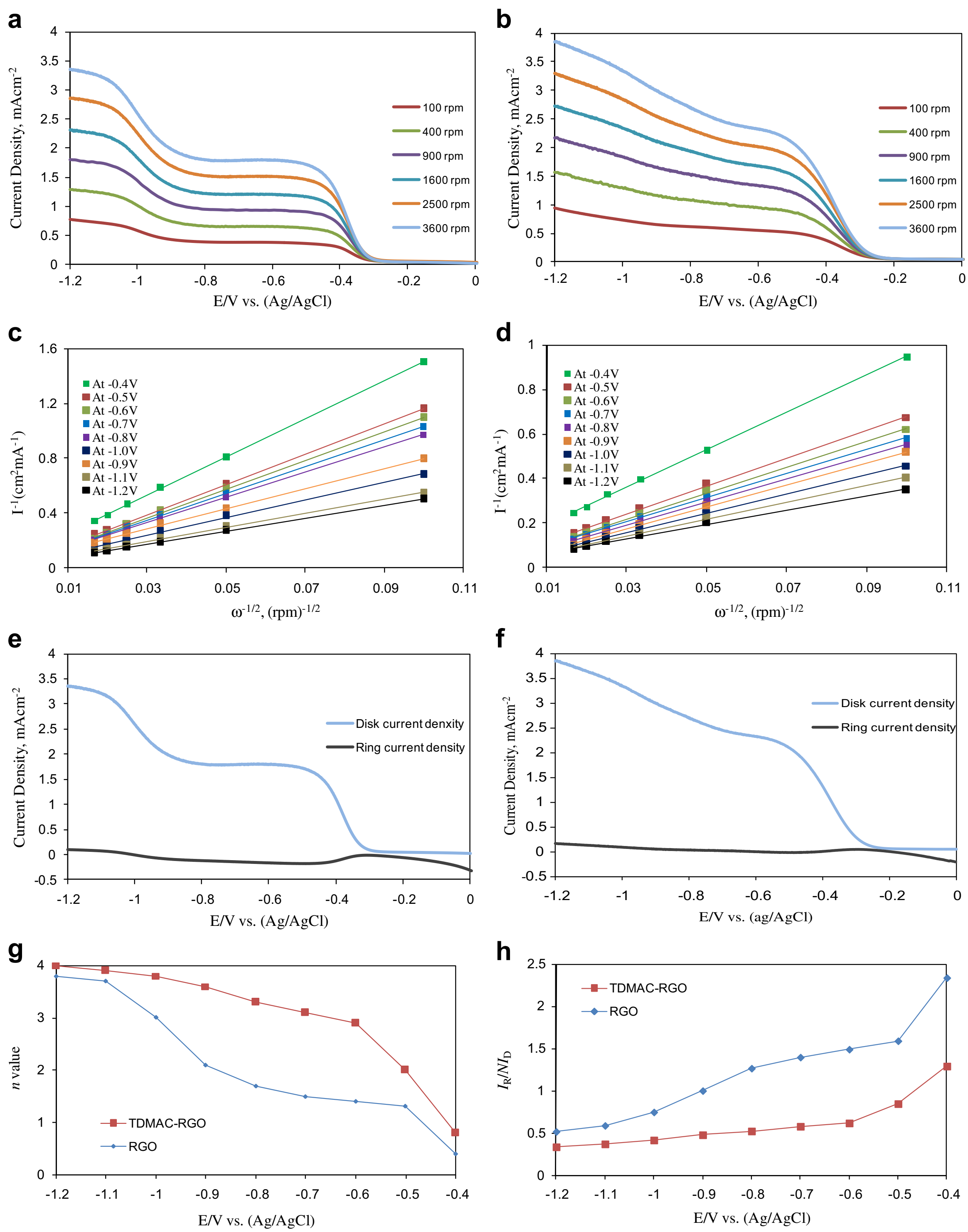

Fig. 5. LSV at different rotation speeds for ORR with RGO (a) and TDMAC-RGO (b) in O_2-saturated 0.1 M KOH at a scan rate of 10 mV s^{-1}; Koutecky–Levich plots for RGO (c) and TDMAC-RGO (d) at different electrode potentials; the RRDE for ORR at RGO (e) and TDMAC-RGO (f) in O_2-saturated 0.1 M KOH at a scan rate of 10 mV s^{-1}, the ring electrode potential was constant at 1.2 V; the dependence of the transferred electron number (g) and the I_R/NI_D ratio with the disk electrode potential for RGO and TDMAC-RGO (h).

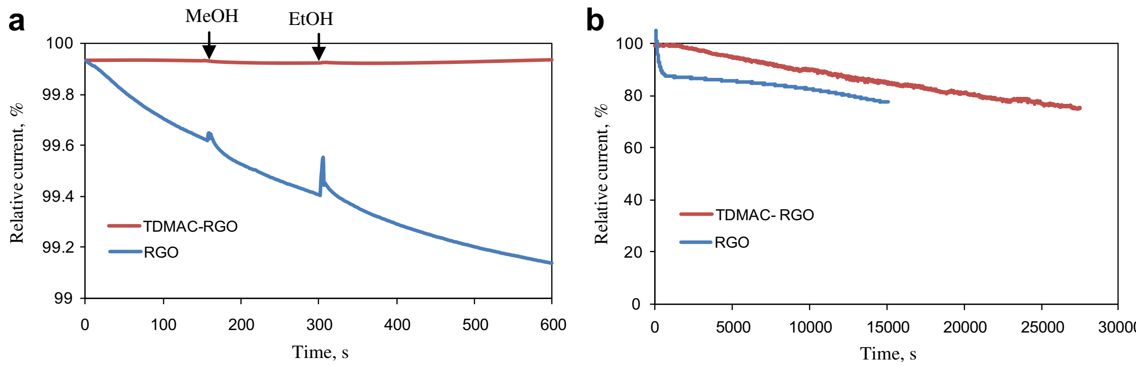

Fig. 6. The current vs. time chronoamperometric responses on the RGO and TDMAC-RGO in O_2 saturated 0.1 M KOH, MeOH and EtOH were added at around 150s and 300s, respectively (a); long term stability (b) at −0.3 V at 1,000 rpm.

of TDMAC-RGO is greater than that of TDMAC unfunctionalized RGO. It is undoubted that the adsorption of TDMAC plays a key role for ORR activity enhancement of RGO.

To gain further insight into the role of the TDMAC-RGO catalyst during the ORR electrochemical process, we continued to compare its electrocatalytic performance with that of the unfunctionalized RGO by linear sweep voltammetry (LSV) in an aqueous solution of O_2-saturated 0.1 M KOH at various rotation rates and a scan rate of 10 mV s^{-1}. The same amount of each catalyst (0.01 mg) was loaded onto a GC rotating-disk electrode (RDE). Fig. 5a and b show the LSV curves at various different rotation rates for RGO- and TDMAC-RGO-modified electrodes, respectively. A potential region where the ORR is under a mix of kinetic-diffusion control and well-defined diffusion-limiting currents was recorded. The onset potential of the TDMAC-RGO electrode for the ORR at approximately − 0.24 V is significantly higher than that of the RGO electrode at about −0.3 V; the ORR limiting current density of the TDMAC-RGO-modified electrode is always larger than that of the RGO electrode at any constant rotation rate.

The Koutecky–Levich plots (I^{-1} vs.$^{-1/2}$) at different electrode potentials displayed good linearity (Fig. 5c and d), which suggests that the electron transfer numbers are similar for oxygen reduction at different electrode potentials. The transferred electron number (n) per O_2 molecule involved has calculated on the basis of the Koutecky–Levich equation (i) [41] as given below:

$$1/I = 1/I_k + 1/\left(0.6nFCD^{2/3}\nu^{-1/6}\omega^{1/2}\right) \quad \text{(i)}$$

where I is the measured current density, I_k is the kinetic current density of the ORR, n is the overall number of electrons transferred during the oxygen reduction, F is the Faraday constant (96,485 C mol^{-1}), C is the bulk concentration of O_2 (1.2 mMl^{-1}), D is the diffusion coefficient of O_2 in the 0.1 M KOH solution (1.9×10^{-5} cm^2s^{-1}), ν is the kinetic viscosity of the electrolyte (1×10^{-2} cm^2s^{-1}) [12], and is the rotating rate (rpm).

Fig. 5e and f show a sample set of ring-disk measurements in RRDE experiments at the RGO and TDMAC-RGO, respectively. The ring currents were used to estimate the amount of generated peroxide ions [14,42]. For TDMAC-RGO, the ring currents amount to negligible fractions of the disk currents in the potential region of −0.24 V and below, in contrast to RGO. This indicates that the ORR has less peroxide production in solution throughout the potential region for O_2 reduction with TDMAC-RGO.

The n values per O_2 molecule are shown in Fig. 5g, in which the n values were found to be dependent on the potential for both the RGO and TDMAC-RGO electrodes. The electron transfer number increased with a decrease in the negative potential. The electron transfer number for ORR at the TDMAC-RGO electrode is always higher than that on the RGO electrode over the potential range covered in this study. Within the range of the electron transfer number from 3 to 4, the oxygen reduction reaction proceeds *via* a nearly four-electron pathway [3,43]. According to Ohsaka and his team [44], when I_R (ring current) is close to 0 and the ratio of I_R/NI_D is 1 (N is the experimental collection efficiency and I_D is the disk current), the transferred electron number can be 4 and 2, respectively. Fig. 5h demonstrates the variation of the ratio I_R/NI_D vs. the disk electrode potentials. As can be seen in this Fig. 5h, the range of the I_R/NI_D values are close to 0 and 1 at the TDMAC-RGO and RGO electrodes, respectively. This evaluation also suggests a four-electron pathway.

The TDMAC functionalized RGO electrode was further exposed to fuel molecules *via* a chronoamperometric method. For direct methanol and/or ethanol fuel cells, the crossover effect of other fuel molecules (*e.g.*, methanol, ethanol) should be considered, because these molecules fed to the anode sometimes permeate through the membrane to the cathode and seriously affect the performance of the cathode catalyst [3,45]. Good ORR catalysts should be inert to fuel molecules oxidation; though, unexpectedly, traditional Pt–C catalysts are highly active to methanol [14]. Fig. 6a illustrates that after the addition of 3 M methanol and ethanol at around 150 s and 300 s, respectively, to O_2-saturated 0.1 M KOH solution at −0.3 V and at a rotation speed of 1,000 rpm, the TDMAC-RGO exhibits excellent selectivity in ORR, with no visible response to methanol/ethanol oxidation. In contrast, RGO exhibits methanol/ethanol oxidation sensitivity with a drastic current decrease with respect to time.

The durability of the catalyst was also evaluated. The catalyst was held at −0.30 V for 28,000 s in an O_2-saturated 0.1 M KOH solution. From Fig. 6b, it can be seen that the chronoamperometric response for TDMAC-RGO exhibits very slow decrease, and a high relative current of approximately 75% (percent) still persisted after 28,000 s. In contrast, the RGO electrode exhibits a gradual decrease with the same current loss after only 15,000 s. These results confirm that TDMAC-RGO has potential for use in alkaline fuel cells. Nevertheless, commercial Pt–C catalyst losses of more than 30% even in short durations has been reported [15,19].

4. Conclusion

In summary, quaternary TDMAC functionalized/adsorbed graphene sheets have been synthesized by a physicochemical approach. After successful adsorption of TDMAC onto the RGO, the resulting TDMAC-RGO exhibits an enhanced catalytic activity towards oxygen reduction as an efficient metal-free electrocatalyst through intermolecular charge-transfer. The reaction kinetics study

confirms that the oxygen reduction in TDMAC-RGO follows a four-electron pathway with excellent long-term stability, and tolerance to cross-over effects of methanol/ethanol in the ORR in an alkaline medium. This type of material will provide an opportunity to develop various metal-free, low-cost, and environmentally friendly efficient ORR catalysts, which are essential for practical applications in fuel cells.

Acknowledgments

This research has supported by the National Research Foundation of Korea (NRF) funded by the Ministry of Education, Science and Technology (2010–0007864).

References

[1] B.C.H. Steele, A. Heinzel, Nature 414 (2001) 345–352.
[2] P. Gong, F. Du, Z.H. Xia, M. Durstock, L. Dai, Science 323 (2009) 760–764.
[3] R. Liu, D. Wu, X. Feng, K. Mullen, Angew. Chem. Int. Ed. 49 (2010) 2565–2569.
[4] J. Zhang, H.Z. Yang, J.Y. Fang, S.H. Zou, Nano Lett. 10 (2010) 638–644.
[5] J. Zhang, K. Sasaki, E. Sutter, R.R. Adzic, Science 315 (2007) 220–222.
[6] B. Lim, M.J.P. Jiang, E.C. Cho, J. Tao, X.M. Lu, Y.M. Zhu, Y.N. Xia, Science 324 (2009) 1302–1305.
[7] Z.W. Chen, M. Waje, W.Z. Li, Y.S. Yan, Angew. Chem. Int. Ed. 46 (2007) 4060–4063.
[8] M. Winter, R.J. Brodd, Chem. Rev. 104 (2004) 4245–4269.
[9] X. Yu, S. Ye, J. Power Sources 172 (2007) 145–154.
[10] K. Gong, F. Du, Z. Xia, M. Dustock, L. Dai, Science 323 (2009) 760–764.
[11] W. Chen, J.M. Kim, S.H. Sun, S.W. Chen, J. Phys. Chem. C 112 (2008) 3891–3898.
[12] W. Chen, S.W. Chen, Angew. Chem. Int. Ed. 48 (2009) 4386–4389.
[13] Y.Y. Shao, J. Liu, Y. Wang, Y.H. Lin, J. Mater. Chem. 19 (2009) 46–59.
[14] L. Qu, Y. Liu, J.B. Baek, L. Dai, ACS Nano 4 (2010) 1321–1326.
[15] Z. Yang, Z. Yao, G. Li, G. Fang, H. Nie, Z. Liu, X. Zhou, X. Chen, S. Huang, ACS Nano 6 (2012) 205–211.
[16] K.S. Novoselov, A.K. Geim, S.V. Morozov, D. Jiang, Y. Zhang, S.V. Dubonos, I.V. Grigorieva, A.A. Firsov, Science 306 (2004) 666–669.
[17] A.J. Patil, J.L. Vickery, T.B. Scott, S. Mann, Adv. Mater. 21 (2009) 3159–3164.
[18] C.H. Lu, H.H. Yang, C.L. Zhu, X. Chen, G.N. Chen, Angew. Chem. Int. Ed. 48 (2009) 4785–4787.
[19] S. Wang, D. Yu, L. Dai, D.W. Chang, J.B. Baek, ACS Nano 8 (2011) 6202–6209.
[20] A.K. Geim, K.S. Novoselov, Nat. Mater. 6 (2007) 183–191.
[21] M.D. Stoller, S.J. Park, Y.W. Zhu, J.H. An, R.S. Ruoff, Nano Lett. 8 (2008) 3498–3502.
[22] H. Wang, J.T. Robinson, X. Li, H. Dai, J. Am. Chem. Soc. 131 (2009) 9910–9911.
[23] C. Berger, Z. Song, T. Li, X. Li, A.Y. Ogbazghi, R. Feng, Z. Dai, A.N. Marchenkov, E.H. Conrad, P.N. First, W.A. de Heer, J. Phys. Chem. B 108 (2004) 19912–19916.
[24] Y. Xu, Z. Liu, X. Zhang, Y. Wang, J. Tian, Y. Huang, Y. Ma, X. Zhang, Y. Chen, Adv. Mater. 21 (2009) 1275–1279.
[25] H. Bai, Y. Xu, L. Zhao, C. Li, G. Shi, Chem. Commun. 13 (2009) 1667–1669.
[26] J. Shen, Y. Hu, C. Li, C. Qin, M. Shi, M. Ye, Langmuir 25 (2009) 6122–6128.
[27] R. Hao, W. Qian, L. Zhang, Y. Hou, Chem. Commun. 48 (2008) 6576–6578.
[28] Q. Liu, A. Ishibashi, T. Fujigaya, K. Mimura, T. Gotou, K. Uera, N. Nakashima, Carbon 49 (2011) 3424–3429.
[29] J. Shen, Y. Hu, M. Shi, X. Lu, C. Qin, C. Li, M. Ye, Chem. Mater. 21 (2009) 3514–3520.
[30] G. Eda, G. Fanchini, M. Chhowalla, Nat. Nanotechnol. 3 (2008) 270–274.
[31] X. Gao, J. Jang, S. Nagase, J. Phys. Chem. C 114 (2009) 832–842.
[32] L.L. Zhang, R. Zhou, X.S. Zhao, J. Mater. Chem. 20 (2010) 5983–5992.
[33] W.S. Hummers, R.E. Offeman, J. Am. Chem. Soc. 80 (1958) 1339. 1339.
[34] H.L. Guo, X.F. Wang, Q.Y. Qian, F.B. Wang, X.H. Xia, ACS Nano 3 (2009) 2653–2659.
[35] A.M. Rao, P.C. Eklund, S. Bandow, A. Thess, R.E. Smalley, Nature 388 (1997) 257–259.
[36] M.-C. Hsiao, S.-H. Liao, M.-Y. Yen, P.-I. Liu, N.-W. Pu, C.-A. Wang, C.-C.M. Ma, ACS Appl. Mater. Interfaces 2 (2010) 3092–3099.
[37] O. Akhavan, E. Ghaderi, J. Phys. Chem. C 113 (2009) 20214–20220.
[38] K.M. Watling, J.F. Parr, L. Rintoul, C.L. Brown, L.A. Sullivan, Spectochim Acta Part A 80 (2011) 106–111.
[39] L.S. Panchakarla, K.S. Subrahmanyam, S.K. Saha, A. Govindaraj, H.R. Krishnamurthy, U.V. Waghmare, C.N.R. Rao, Adv. Mater. 21 (2009) 4726–4730.
[40] S. Wang, F. Yang, S.P. Jiang, S. Chen, X. Wang, Electrochem. Commun. 12 (2010) 1646–1649.
[41] U.A. Paulus, A. Wokaun, G.G. Scherer, T.J. Schmidt, V. Stamenkovic, V. Radmilovic, N.M. Markovic, P.N. Ross, J. Phys. Chem. B 106 (2002) 4181.
[42] K. Gong, F. Du, Z. Xia, M. Durstock, L. Dai, Science 323 (2009) 760–764.
[43] G. Jurmann, K. Tammeveski, J. Electroanal. Chem. 597 (2006) 119–126.
[44] M.S.E. Deab, T. Sotomura, T. Ohsaka, Electrochem. Commun. 7 (2005) 29–34.
[45] A. Hamnett, in: W. Vielstich, A. Lamm, H. Gasteiger (Eds.), Handbook of Fuel Cells: Fundamentals, Technology and Applications, vol. 1, John Wiley & Sons, Ltd., New York, 2003, p. 305.